


# The different impacts of g-C<sub>3</sub>N<sub>4</sub> nanosheets on PVDF and PSF ultrafiltration membranes for Remazol black 5 dye rejection

Dilek Senol-Arslan<sup>1</sup>  | Ayse Gul<sup>2</sup> | Nadir Dizge<sup>3</sup> | Kasim Ocakoglu<sup>4</sup> | Nigmet Uzal<sup>2</sup>

<sup>1</sup>Abdullah Gül University, Department of Nanotechnology Engineering, Kayseri, Turkey

<sup>2</sup>Abdullah Gül University, Department of Civil Engineering, Kayseri, Turkey

<sup>3</sup>Mersin University, Department of Environmental Engineering, Mersin, Turkey

<sup>4</sup>Tarsus University, Department of Engineering Fundamental Sciences, Tarsus, Turkey

## Correspondence

Dilek Senol-Arslan, Abdullah Gül University, Department of Nanotechnology Engineering, Kayseri 38380, Turkey.  
Email: [dilek.senol@agu.edu.tr](mailto:dilek.senol@agu.edu.tr)

Nigmet Uzal, Abdullah Gül University, Department of Civil Engineering, Kayseri 38380, Turkey.  
Email: [nigmet.uzal@agu.edu.tr](mailto:nigmet.uzal@agu.edu.tr)

## Abstract

Membranes combined with nanoparticles are an excellent combination capable of successfully removing various contaminants, such as dyes from wastewater while using very little energy and decreasing pollution. The present study reports an efficient approach for Remazol Black 5 (RB5) dye removal using composite graphitic carbon nitride nanosheets (g-C<sub>3</sub>N<sub>4</sub>), polysulfone (PSF), and polyvinylidene fluoride (PVDF) membranes. The membranes were prepared using the phase inversion method, with varying quantities of g-C<sub>3</sub>N<sub>4</sub> nanosheets ranging from 0.1%, 0.2% to 0.3%. The prepared g-C<sub>3</sub>N<sub>4</sub> nanosheets were characterized by FTIR, SEM analyses, and zeta potential measurements. FTIR and SEM studies, contact angle, water permeability, COD, and dye rejection measurements were used to characterize the g-C<sub>3</sub>N<sub>4</sub> nanosheets embedded in PSF and PVDF membranes. After the addition of 0.3 wt% g-C<sub>3</sub>N<sub>4</sub>, the water flux of the 0.3 wt% g-C<sub>3</sub>N<sub>4</sub> embedded PSF membrane was the highest, whereas the water flux of the 0.3 wt% g-C<sub>3</sub>N<sub>4</sub> embedded PVDF membrane was the lowest. The ultrafiltration (UF) membrane's performance with g-C<sub>3</sub>N<sub>4</sub> embedded showed an RB5 rejection rate of more than 80% and a COD removal efficiency of more than 45%. The results of the experimental filtration showed that RB5 rejection reached maximum values of 91.3% for 0.1 wt% g-C<sub>3</sub>N<sub>4</sub>/PSF, and 85.6% for 0.3 wt% g-C<sub>3</sub>N<sub>4</sub>/PVDF.

## KEYWORDS

g-C<sub>3</sub>N<sub>4</sub> nanosheets, PSF membrane, PVDF membrane, Remazol black 5 dye rejection, ultrafiltration

## 1 | INTRODUCTION

Currently, the effects of air pollution, water pollution, global warming from fossil fuels, deforestation, irresponsible waste

disposal, plastic pollution, and climate change are being felt both locally and globally. At this point, nanotechnology is among the most significant technological developments of the 21st century for solving modern-day problems.

This is an open access article under the terms of the [Creative Commons Attribution-NonCommercial-NoDerivs](https://creativecommons.org/licenses/by-nc-nd/4.0/) License, which permits use and distribution in any medium, provided the original work is properly cited, the use is non-commercial and no modifications or adaptations are made.

© 2023 The Authors. *Journal of Applied Polymer Science* published by Wiley Periodicals LLC.

Nanotechnology is a significant technological advancement in science, technology, and business, and it is probably used in all relevant industries and fields, including engineering, agriculture, medicine, physics, chemistry, and biology, as well as in electrical appliances, water purifiers, energy, environmental protection, resource management, and many other areas. Nanotechnology is used to create systems and has significant applications in solving environmental problems, such as the creation of nanomaterials, nanotubes, nanocomposites, nanofilters, and nanoparticles.<sup>1,2</sup> In addition, it is being used to create energy that will eventually replace traditional fossil fuels. They have been utilized to produce and store energy thanks to their catalytic activity, optical characteristics, and surface features. Due to their unique structure and characteristics, nanomaterials play a significant role in the uptake and storage of hydrogen. Recently, there has been a noticeable growth in the usage of nanotechnology for hydrogen storage.<sup>3-8</sup>

The use of nanotechnology makes it possible to reduce many air pollutants in cities and industries to a reasonable level, treat industrial and urban effluents in the best possible way to prevent water pollution, and minimize soil pollutants. The technology of nano remediation is an effective solution for the prevention, monitoring, detection, and remediation of pollutants in the environment.<sup>9-11</sup>

A variety of nanostructured compounds can be easily prepared in very mild conditions with low energy consumption and preparation costs without causing environmental pollution, and for effective treatment of contaminated water under sunlight thanks to the design and presentation of methods based on green chemistry.<sup>12,13</sup>

Numerous nanostructured have been used as photocatalysts to date in order to remove environmental pollutants and remediate effluents that contain hazardous organic materials.<sup>1,14</sup>

Textile dyeing wastewaters are the most difficult industrial wastewaters to treat because they contain a high concentration of hazardous contaminants, including azo dyes and inorganic salts. Reactive Black 5 (RB5), also known as Remazol Black B in the textile industry, has been the most popular reactive dye, accounting for 50% of the market demand for reactive dyes.<sup>15</sup> It is popular due to its low price, low energy usage, vibrant colors, and high stability.<sup>16</sup>

Due to the aromatic rings in their composition, the majority of dyes are toxic, mutagenic, and carcinogenic, limiting aquatic photosynthesis, and reducing dissolved oxygen levels, hence causing toxicity in plants, animals, and humans.<sup>17-21</sup> The global community is concerned about the possible negative effects of wastewater dyeing on aquatic ecosystems, which is a threat to the environment, and the largest source is organic dyes. Therefore, it is crucial to utilize the appropriate methods for removing these dyes from aquatic systems.<sup>21-24</sup>

For the removal of toxic organic dyes, conventional water treatment technologies such as adsorption,<sup>25</sup> photocatalysis degradation,<sup>26</sup> coagulation,<sup>27</sup> and membrane technology are utilized.<sup>28</sup> Membrane technology is favored over other wastewater treatment methods due to its excellent filtration, low energy consumption, ease of scaling up and operation, and eco-friendly and renewable approach.<sup>21,29</sup>

Membranes are produced commercially from polyvinyl alcohol (PVA), polyvinylidene fluoride (PVDF), polyamide (PA), polyacrylic acid (PAA), polytetrafluoroethylene (PTFE), polyimide (PI), cellulose acetate (CA), polysulfone (PSF), and other low-cost polymers.<sup>30</sup> When compared to other polymeric materials, polyvinylidene fluoride (PVDF) and polysulfone (PSF) have higher mechanical strength, stability, and, thermal, and chemical stability, which has attracted the attention of many researchers. PSF is resistant to a wide range of temperatures and pH, and it also has good film-forming characteristics.<sup>31,32</sup>

Despite the benefits of membrane filtration technologies, separation performance is limited due to their durability, fouling resistance/pressure, and trade-off between water flux and selectivity. Enhanced membranes have been created using nanoparticles such as SiO<sub>2</sub>,<sup>33</sup> Al<sub>2</sub>O<sub>3</sub>,<sup>34</sup> ZrO<sub>2</sub>,<sup>35</sup> clay,<sup>36</sup> carbon nanotubes (CNTs),<sup>37</sup> graphene,<sup>38</sup> TiO<sub>2</sub>,<sup>39</sup> ZnO,<sup>40</sup> and graphitic carbon nitride (g-C<sub>3</sub>N<sub>4</sub>)<sup>41</sup> to address the inherent drawbacks of existing membrane technologies, such as providing additional hydrophilic groups to the membrane surface, increasing membrane hydrophilicity, and improving antifouling capabilities.<sup>41</sup>

As a graphite analog, graphitic carbon nitride (g-C<sub>3</sub>N<sub>4</sub>) has a layered 2D structure that may be described as a nitrogen atom replaced graphite special framework with  $\pi$ -conjugated graphite structure created by carbon and nitrogen sp<sup>2</sup> hybridization.<sup>42</sup> g-C<sub>3</sub>N<sub>4</sub> has gained a lot of attention due to its abundance of raw materials, porous features, distinctive energy band, and simplicity of synthesis, chemical stability, lack of toxicity, metal-free nature, and environmental friendliness. It has a laminar structure with multiple nanopores that may operate as water transport channels and act as a molecular sieve, making it ideal for membrane separation.<sup>23,43</sup>

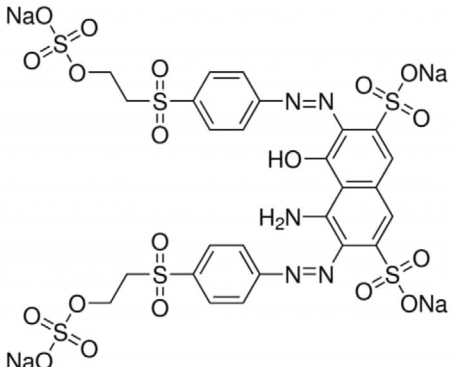
The main novelty of the study is to investigate the effect of g-C<sub>3</sub>N<sub>4</sub> on PVDF and PSF ultrafiltration (UF) membranes for RB5 dye rejection.

## 2 | MATERIALS AND METHODS

### 2.1 | Materials

PVDF and PSF (with an average  $M_w = 60,000$  Da) were supplied from Acros Organics (Geel, Belgium), NMP and DMF were obtained from Merck (Darmstadt, Germany). Zinc nitrate hexahydrate (Zn(NO<sub>3</sub>)<sub>2</sub>·6H<sub>2</sub>O > 99%), urea

TABLE 1 Chemical structures of RB 5.

Empirical formula C <sub>26</sub> H <sub>21</sub> N <sub>5</sub> Na <sub>4</sub> O <sub>19</sub> S <sub>6</sub>	
Molecular weight	991.82 g/Mol
λ <sub>max</sub>	598 nm
Class	Textile azo dyes
Structure	

(CH<sub>4</sub>N<sub>2</sub>O > 99.5%), and ammonium hydroxide solution (NH<sub>4</sub>OH, 26%) were purchased from Sigma-Aldrich (USA). All chemicals used in this work were of analytical grade and used without further purification. RB5, which was used as a model pollutant purchased from Sigma-Aldrich (USA). Some physicochemical properties are given in Table 1. The RB5 was chosen for membrane filtration treatment because of its widely used in the textile sector. 1 g of RB 5 dye was dissolved in 1 L of distilled water to make a stock solution. The desired concentration of RB5(10, 30, 50, 70, and 100 mg/L) was prepared by dilution of the stock solution using distilled water. The reason for choosing these concentrations is due to discharge from effluents of textile industries in the range of 10–100 ppm.<sup>2</sup>

## 2.2 | Synthesis of g-C<sub>3</sub>N<sub>4</sub>

Graphite-like g-C<sub>3</sub>N<sub>4</sub> nanosheets were synthesized based on the procedure described previously in the literature.<sup>44</sup> 50 g of urea was first calcinated at 580°C for 3 h at a heating rate of 5°C/min under argon gas flow in the one-step synthesis technique. The material was cooled around at ±25°C, washed with HNO<sub>3</sub> solution (0.1 mol/L) and water, and dried at 70°C overnight.

## 2.3 | Membrane fabrication

All four types of membranes pristine PSF, pristine PVDF, PSF/g-C<sub>3</sub>N<sub>4</sub>, and PVDF/g-C<sub>3</sub>N<sub>4</sub> membranes were fabricated based upon the phase inversion method.<sup>33</sup> 20 wt%

PSF and 17 wt% PVDF membranes were fabricated for three different concentrations of g-C<sub>3</sub>N<sub>4</sub> (0.1, 0.2, and 0.3 wt%). The viscous membrane solutions were stirred at 500 rpm for 24 h ambient temperature as 25 ± 1°C. Then, all the solutions were sonicated for 15 min to remove air bubbles. A schematic illustration of the membrane fabrication is presented in Figure 1.

## 2.4 | Dead-end filtration experiments

A dead-end stirred cell filtration system (Sterlitech, HP4750, USA) with an effective membrane area of 14.6 cm<sup>2</sup> and a 300 mL volume capacity was used to test the membranes' filtration performance. The reservoir was filled with 250 mL of distilled water or dye solution, and the membrane samples were placed at the bottom of the reservoir. Nitrogen gas was used to obtain the permeate flux. A schematic illustration of the dead-end stirred cell filtration system is presented in Figure 2.

Distilled water was used to obtain water flux values at a constant trans membrane pressure (TMP) of 10 and 25 bar at 25 ± 1°C. Every 15 min, the water flux was monitored by tracking the volume of filtrate amounts collected. The water fluxes (J, L m<sup>-2</sup> h<sup>-1</sup>) of the pristine PSF, pristine PVDF, PSF/g-C<sub>3</sub>N<sub>4</sub>, and PVDF/g-C<sub>3</sub>N<sub>4</sub> membranes were calculated by Equation (1).

$$J = \frac{V}{A \times \Delta t} \quad (1)$$

where V (L), t (h), and A (m<sup>2</sup>) represent the filtrate volume, operating time, and effective membrane area, respectively.

The dye solution was prepared and loaded into a dead-end stirred cell filtration system with a stirring speed of 250 rpm, which was operated at 10 bar for PVDF membranes and 25 bar for PSF membranes, respectively, at 25 ± 1°C. In the filtration experiments, the original pH of the dye solutions was used. The membrane samples were put into the membrane cell with a total volume of 250 mL containing RB5 in different concentrations. The removal efficiency (RE, %) of the Remazol Black 5 was calculated by Equation (2). The concentrations of RB5 were measured with a UV-Visible spectroscopy at a wavelength of 598 nm.

$$R\% = (1 - C_p) / C_f \times 100 \quad (2)$$

where C<sub>p</sub> (mg/L) and C<sub>f</sub> (mg/L) are the dye concentrations of the solutes in the feed and permeate, respectively.

Chemical oxygen demand (COD) was analyzed according to the Standard Methods (5220 D. Closed

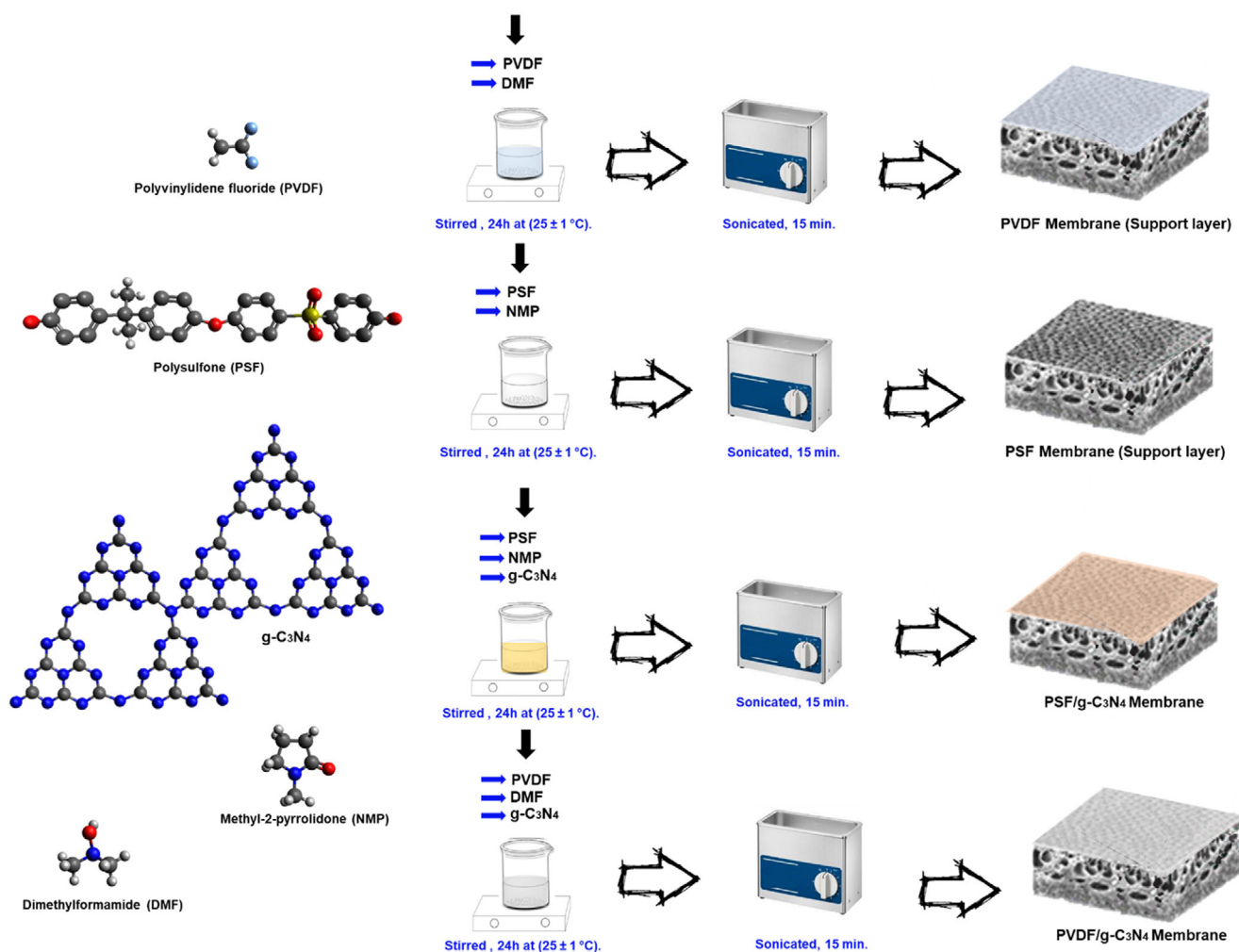


FIGURE 1 A schematic illustration of the membranes' fabrication. [Color figure can be viewed at [wileyonlinelibrary.com](https://onlinelibrary.wiley.com)]

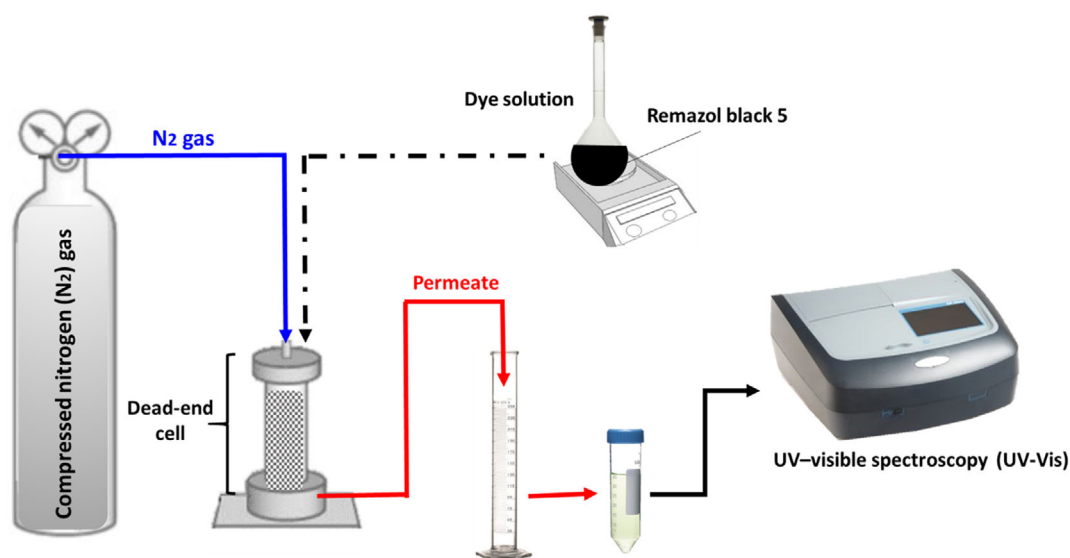


FIGURE 2 A schematic diagram of the dead-end stirred cell filtration system. [Color figure can be viewed at [wileyonlinelibrary.com](https://onlinelibrary.wiley.com)]

Reflux, Colorimetric Method, APHA 2005) and the reactor and spectrophotometer were HACH DR/6000 and HACH DR/200, respectively. The COD was determined using a spectrophotometer at a wavelength of 420 nm. The COD removal efficiency (RE, %) was calculated by Equation (3).

$$R\% = \frac{Y_0 - Y}{Y_0} \times 100 \quad (3)$$

where  $Y_0$  is the initial value of COD and  $Y$  is the final value of COD, respectively.

## 2.5 | Characterization of g-C<sub>3</sub>N<sub>4</sub> nanosheets and composite membranes

The structure and morphology of g-C<sub>3</sub>N<sub>4</sub> nanosheets and g-C<sub>3</sub>N<sub>4</sub> nanosheets embedded composite membranes were examined using a scanning electron microscope (Zeiss Gemini) with a 10 kV applied voltage. FT-IR spectra were used to identify the functional properties of g-C<sub>3</sub>N<sub>4</sub> nanosheets and g-C<sub>3</sub>N<sub>4</sub> embedded composite membranes using an FT-IR spectrometer (Thermo Nicolet Avatar 370).

The contact angle meter (Attention-Theta Lite, Biolin Scientific, Finland) was used to test the surface hydrophilicity of the g-C<sub>3</sub>N<sub>4</sub> embedded composite membranes using the sessile drop method. Zeta potential measurements were performed using Nano ZS90 (Malvern, UK) equipment to study the surface charges of g-C<sub>3</sub>N<sub>4</sub> nanosheets.

## 3 | RESULTS AND DISCUSSION

### 3.1 | Characterization of g-C<sub>3</sub>N<sub>4</sub> nanosheets

Determining the isoelectric point (IEP) of g-C<sub>3</sub>N<sub>4</sub> nanosheets is critical because this value represents the surface charges and provides a reference for the processing of g-C<sub>3</sub>N<sub>4</sub> nanosheets in combination with other compounds in solution. Therefore, zeta potential analyses were carried out between pH 2.5–12. As shown in Figure 3, the zeta potential of g-C<sub>3</sub>N<sub>4</sub> nanosheets has the IEP at pH 4.5, the point at which the zeta potential shifts from positive to negative. The region below g-C<sub>3</sub>N<sub>4</sub> nanosheets' IEP is positively charged as a result of the highest concentration of H<sup>+</sup> ions there. For pH >4.5 the surface charge of g-C<sub>3</sub>N<sub>4</sub> nanosheets is negatively charged due to the highest concentration of OH<sup>-</sup> ions.

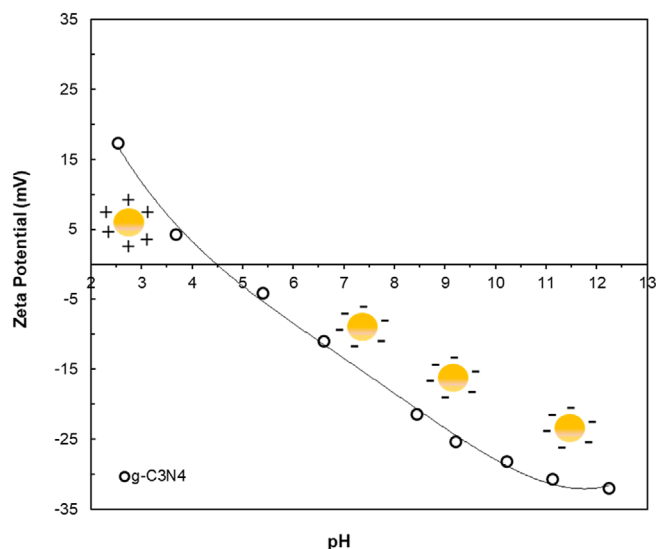


FIGURE 3 The zeta potential of g-C<sub>3</sub>N<sub>4</sub> nanosheets. [Color figure can be viewed at [wileyonlinelibrary.com](https://onlinelibrary.wiley.com/doi/10.1002/app.54514)]

The morphology of g-C<sub>3</sub>N<sub>4</sub> nanosheets as obtained by SEM is shown in Figure 4b. It is observed that the nanosheets show a layered and stacked irregular structure.<sup>42</sup> The cross-sectional image of pristine PVDF and PSF membranes showed finger-like structures in the sub-layer Figure 4a,c. After the different concentrations of the g-C<sub>3</sub>N<sub>4</sub> nanosheets (0.1, 0.2, and 0.3 wt%) were added to the pristine PVDF (Figure 4d) and PSF (Figure 4e) membranes, both of them showed the retraction of densification of the sponge-like layer. The total membrane thickness decreased with the increase in g-C<sub>3</sub>N<sub>4</sub> nanosheet loading.

FT-IR analysis was used to examine the changes in functional groups of the pristine PVDF, PSF membranes and composite membranes (Figure 5a,b).

The main peak for pristine g-C<sub>3</sub>N<sub>4</sub> powder is at 807 cm<sup>-1</sup>, which is attributed to repeating triazine units.<sup>45,46</sup> Some other absorption peaks of g-C<sub>3</sub>N<sub>4</sub> also observed in FTIR are at 1200, and 1637 cm<sup>-1</sup>, which are representatives of C—N and C=N functionalities, respectively.<sup>47,48</sup>

For pristine PVDF, the main peak at 1413 cm<sup>-1</sup> is attributed to the stretching vibrations of C—H. The peaks of g-C<sub>3</sub>N<sub>4</sub>/PVDF composite membranes at 1637 cm<sup>-1</sup> can be related to the C=N stretching vibrational modes of g-C<sub>3</sub>N<sub>4</sub>.<sup>49</sup>

The stretching and deformation vibrations of CH<sub>2</sub> correspond to the maxima at 2979 and 1411 cm<sup>-1</sup>, respectively. Additionally, the stretching vibrations of CF<sub>2</sub> can be responsible for the peak at 1181 cm<sup>-1</sup>.<sup>50</sup>

FT-IR spectra of pristine PSF membrane, the main characteristic peaks at 1294 cm<sup>-1</sup> and correspond to the

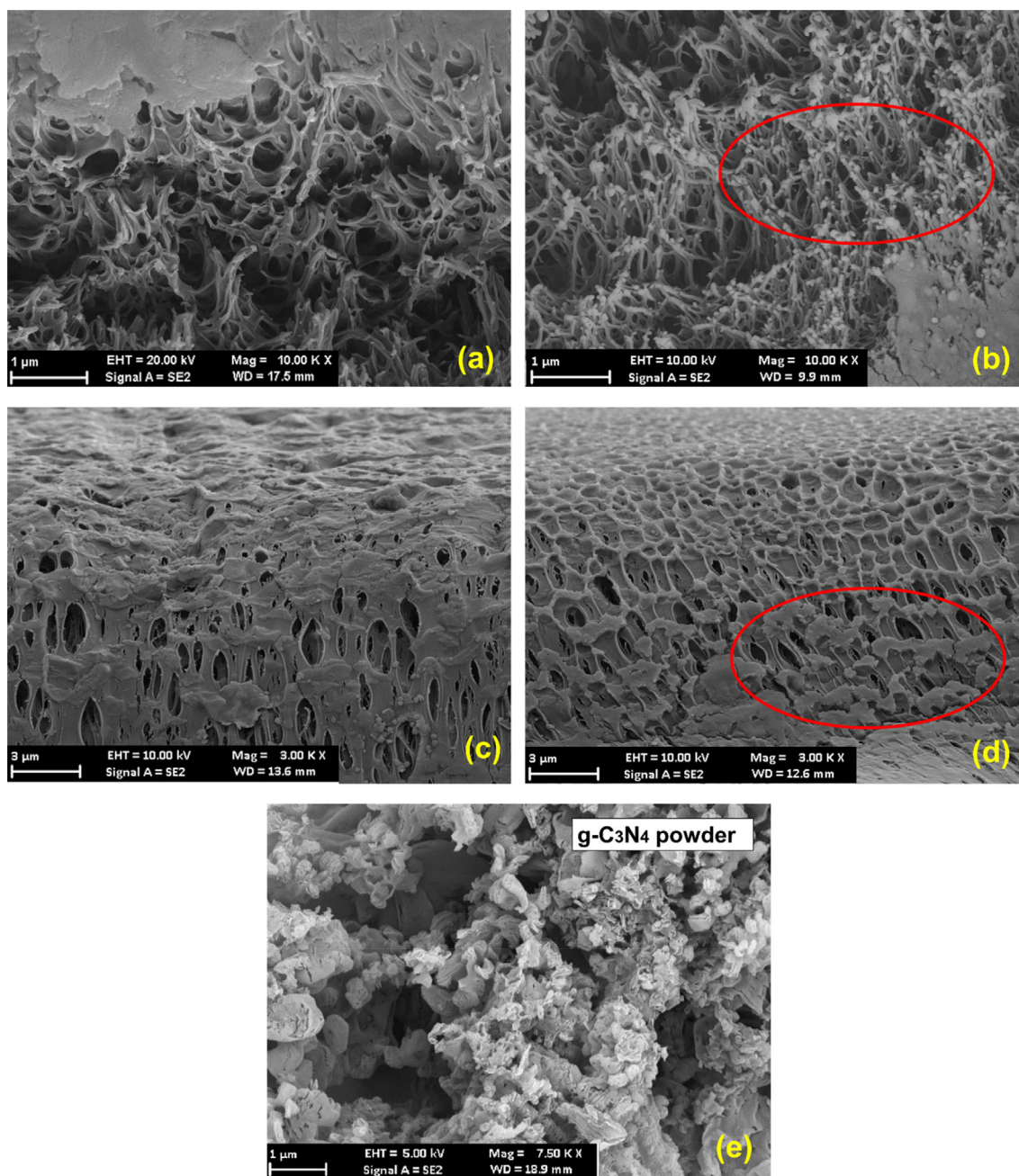


**FIGURE 4** The cross-section SEM images of (a) Pristine PSF membrane, (b) PSF/g-C<sub>3</sub>N<sub>4</sub> membrane (c) Pristine PVDF membrane, (d) PVDF/g-C<sub>3</sub>N<sub>4</sub> membrane and (e) g-C<sub>3</sub>N<sub>4</sub> nanosheets. [Color figure can be viewed at [wileyonlinelibrary.com](https://onlinelibrary.wiley.com/terms-and-conditions)]

O=S=O stretching vibration.<sup>51</sup> The adsorption band at 1323 cm<sup>-1</sup> is attributed to C=N stretching.<sup>52</sup>

The fabricated g-C<sub>3</sub>N<sub>4</sub> embedded composite PVDF and PSF membranes at three different concentrations exhibited similar and comparable FTIR spectra to pristine PVDF and PSF membranes, as displayed in Figure 5a,b.

Figures 6 and 7 show before and after RB5 dye rejection of PVDF and PSF membranes fabricated at three different concentrations. SEM images were taken to determine the influence of g-C<sub>3</sub>N<sub>4</sub> nanosheets on the rejection of RB5.

The RB5 dye molecules smooth the membrane surface. This situation tells us that there is a surface complexation between the membrane surface and the RB5 dye molecules. This is evidence of the adsorption behavior of RB5 on PVDF and PSF membranes in terms of surface areas and pore sizes.

The contact angle is used to determine whether the membrane surface is hydrophilic or hydrophobic. A low contact angle value implies hydrophilicity. The contact angles of the prepared membranes outer surfaces (pristine PSF and pristine PVDF, three various PVDF/g-C<sub>3</sub>N<sub>4</sub>

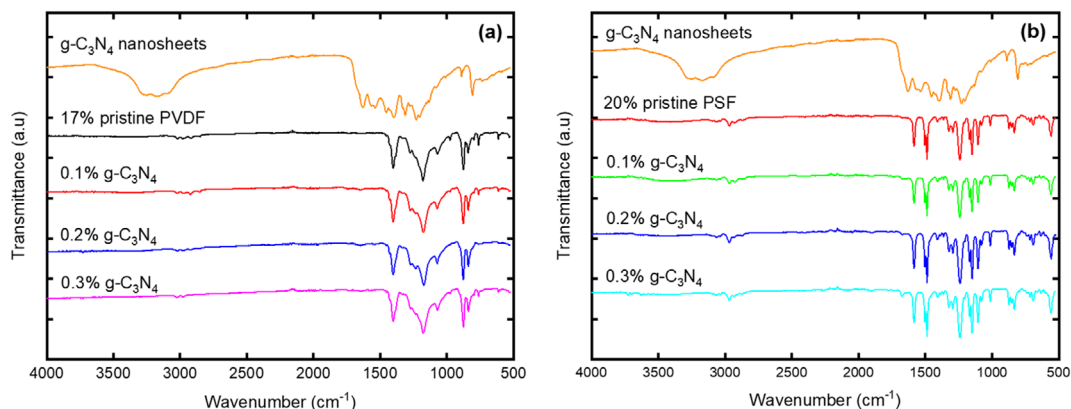


FIGURE 5 (a) FTIR spectra of g-C<sub>3</sub>N<sub>4</sub> nanosheets, 17 wt% pristine PVDF membrane, and g-C<sub>3</sub>N<sub>4</sub> embedded composite membranes at three different concentrations; 0.1 wt% PVDF/g-C<sub>3</sub>N<sub>4</sub>, 0.2 wt% PVDF/g-C<sub>3</sub>N<sub>4</sub>, and 0.3 wt% PVDF/g-C<sub>3</sub>N<sub>4</sub>. (b) FTIR spectra of g-C<sub>3</sub>N<sub>4</sub> nanosheets, 20 wt% PSF membrane, and the g-C<sub>3</sub>N<sub>4</sub> embedded membranes at three different concentrations; 0.1 wt% PSF/g-C<sub>3</sub>N<sub>4</sub>, 0.2 wt% PSF/g-C<sub>3</sub>N<sub>4</sub>, and 0.3 wt% PSF/g-C<sub>3</sub>N<sub>4</sub>. [Color figure can be viewed at [wileyonlinelibrary.com](http://wileyonlinelibrary.com)]

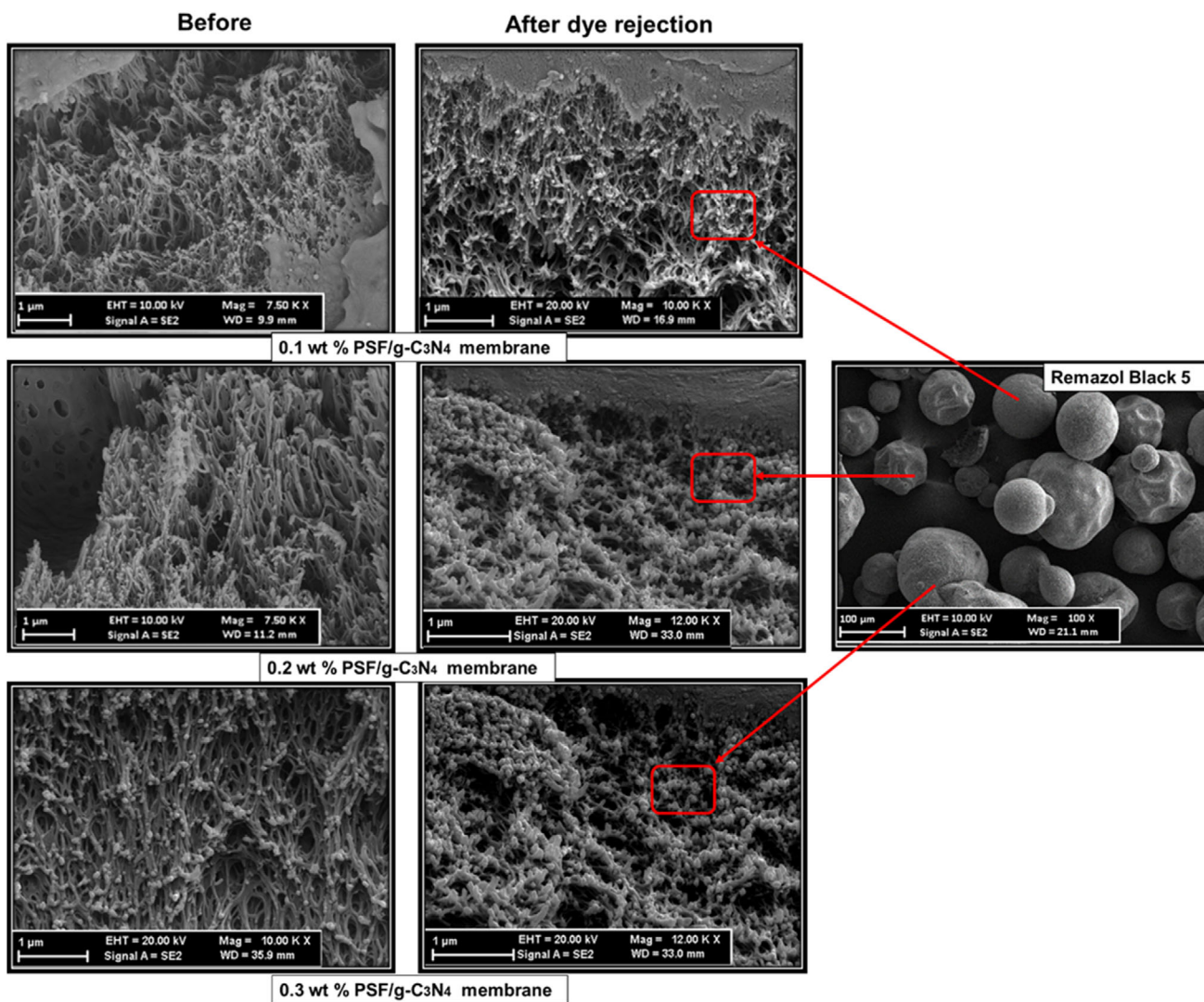


FIGURE 6 SEM images of RB 5, and the cross-section of g-C<sub>3</sub>N<sub>4</sub> embedded membranes at three different concentrations; 0.1 wt% PSF/g-C<sub>3</sub>N<sub>4</sub>, 0.2 wt% PSF/g-C<sub>3</sub>N<sub>4</sub>, and 0.3 wt% PSF/g-C<sub>3</sub>N<sub>4</sub>. [Color figure can be viewed at [wileyonlinelibrary.com](http://wileyonlinelibrary.com)]

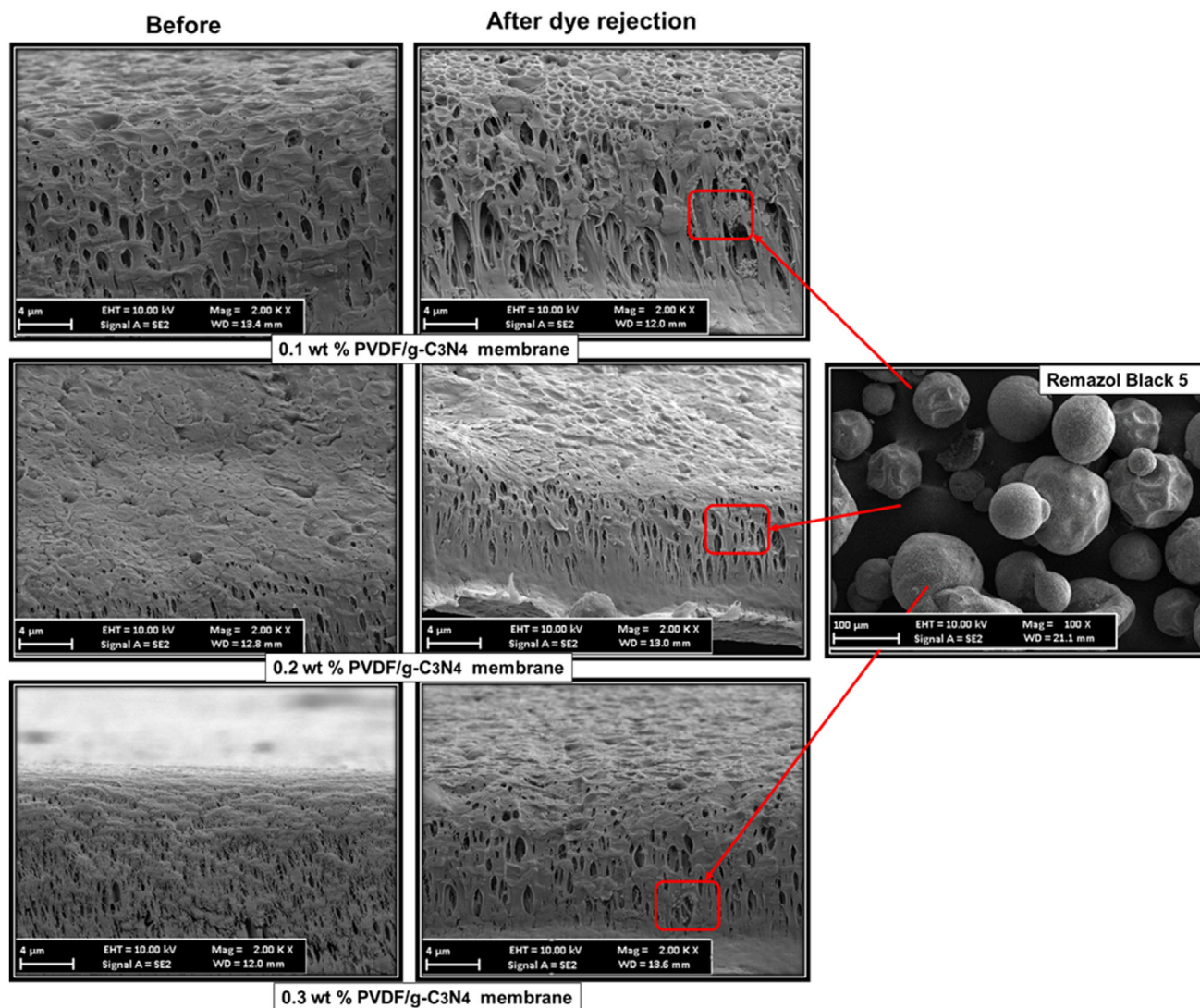


FIGURE 7 SEM images of Remazol Black 5, and the cross-section of g-C<sub>3</sub>N<sub>4</sub> embedded membranes at three different concentrations; 0.1 wt% PVDF/g-C<sub>3</sub>N<sub>4</sub>, 0.2 wt% PVDF/g-C<sub>3</sub>N<sub>4</sub>, and 0.3 wt% PVDF/g-C<sub>3</sub>N<sub>4</sub>. [Color figure can be viewed at [wileyonlinelibrary.com](https://onlinelibrary.wiley.com/doi/10.1002/app.54514)]

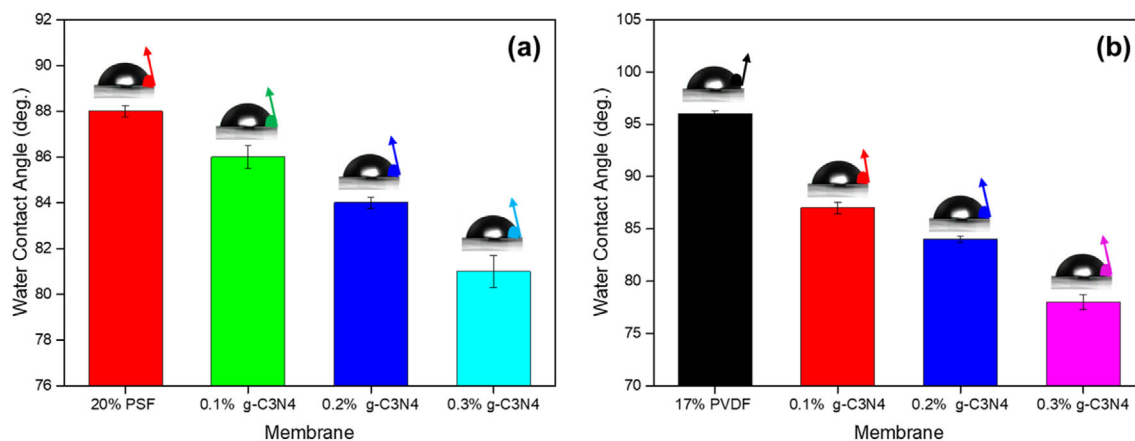
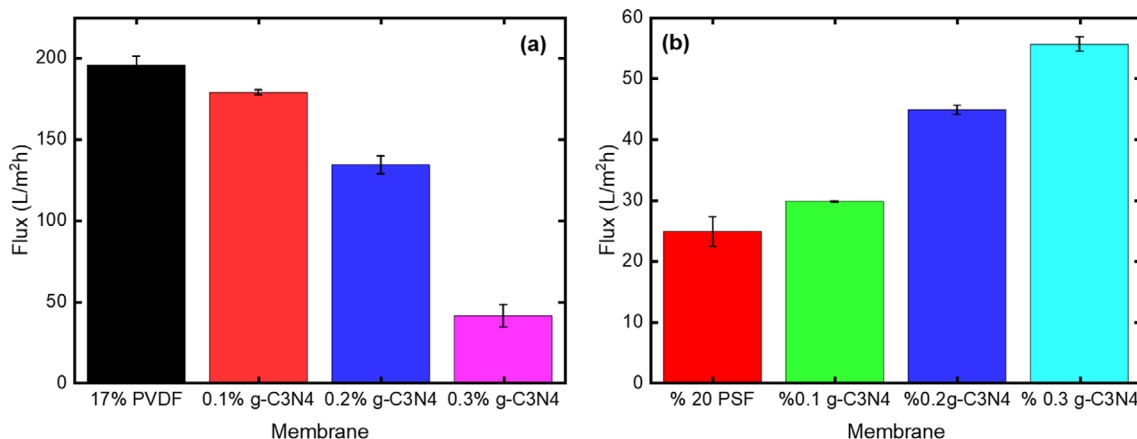


FIGURE 8 Contact angle measurements of (a) 20 wt% PSF; 0.1 wt% g-C<sub>3</sub>N<sub>4</sub>, 0.2 wt% g-C<sub>3</sub>N<sub>4</sub>, and 0.3 wt% g-C<sub>3</sub>N<sub>4</sub> embedded PSF membrane. (b) 17 wt% PVDF; 0.1 wt% g-C<sub>3</sub>N<sub>4</sub>, 0.2 wt% g-C<sub>3</sub>N<sub>4</sub>, and 0.3 wt% g-C<sub>3</sub>N<sub>4</sub> embedded PVDF membrane. [Color figure can be viewed at [wileyonlinelibrary.com](https://onlinelibrary.wiley.com/doi/10.1002/app.54514)]





**FIGURE 9** Pristine water flux of (a) 17 wt% PVDF and three different concentrations of g-C<sub>3</sub>N<sub>4</sub> (0.1 wt%, 0.2 wt%, and 0.3 wt%) embedded membranes. (b) 20 wt% PSF and three different concentrations of g-C<sub>3</sub>N<sub>4</sub> (0.1 wt%, 0.2 wt%, and 0.3 wt%) embedded membranes. [Color figure can be viewed at [wileyonlinelibrary.com](https://onlinelibrary.wiley.com)]

and PSF/g-C<sub>3</sub>N<sub>4</sub> membrane concentrations) were examined in detail (Figure 8a,b). When g-C<sub>3</sub>N<sub>4</sub> nanosheets embedded in membranes compared to pristine PSF membranes, it was seen that, it had a lower water contact angles from 88 to 81° (Figure 8a). PVDF/g-C<sub>3</sub>N<sub>4</sub> membranes were showed a lower water contact angle when compared to the pristine PVDF membrane (Figure 8b). The maximum contact angle for the pristine PVDF membrane was found to be 96° due to its hydrophobic nature. PVDF/g-C<sub>3</sub>N<sub>4</sub> membranes have been observed to reduce the water contact angle up to 78°.

As can be seen in Figure 8 adding g-C<sub>3</sub>N<sub>4</sub> nanosheets to PVDF and PSF membranes can increase their hydrophilicity and reduce their contact angle. This is because g-C<sub>3</sub>N<sub>4</sub> has a unique structure and high surface area, providing large active sites that can interact with water molecules and promote their adsorption. This interaction increases the surface free energy of the g-C<sub>3</sub>N<sub>4</sub>/PVDF and g-C<sub>3</sub>N<sub>4</sub>/PSF membranes and reduces the contact angle.

### 3.2 | Water filtration and rejection of Remazol black 5 dye experiments

The pristine water fluxes of PVDF, PVDF/0.1% g-C<sub>3</sub>N<sub>4</sub>, PVDF/0.2% g-C<sub>3</sub>N<sub>4</sub>, and PVDF/0.3% g-C<sub>3</sub>N<sub>4</sub> were determined at 10 bar using a dead-end filtration system. The results of pristine water flux from membranes are shown in Figure 9a. The pristine water fluxes of PVDF, PVDF/0.1% g-C<sub>3</sub>N<sub>4</sub>, PVDF/0.2% g-C<sub>3</sub>N<sub>4</sub>, and PVDF/0.3% g-C<sub>3</sub>N<sub>4</sub> are 189.9, 177.2, 139.5, and 47.8 L m<sup>-2</sup> h<sup>-1</sup>, respectively. As can be seen, the water flux for PVDF/g-C<sub>3</sub>N<sub>4</sub> membrane decreased from 177.2 to 47.8 L m<sup>-2</sup> h<sup>-1</sup> by the addition of g-C<sub>3</sub>N<sub>4</sub> from 0.1% to 0.3%, a significant

decrease (73.1%) in flux is achieved as a result of a compact layer that has formed on the PVDF substrate, blocking the passage of water molecules.<sup>31</sup> Huang et al. discovered a similar outcome: the pure water flux of the modified membranes (MCU-C<sub>3</sub>N<sub>4</sub>/PVDF) reduced as the MCU-C<sub>3</sub>N<sub>4</sub> concentration was raised. (Huang et al., Evaluation of self-cleaning and photocatalytic properties of modified g-C<sub>3</sub>N<sub>4</sub> based PVDF membranes driven by visible light.<sup>53</sup> Hasanzade (2021) found that PVDF/g-C<sub>3</sub>N<sub>4</sub>/Chitosan and PVDF/g-C<sub>3</sub>N<sub>4</sub> membranes have lower pristine water flux than pristine PVDF.<sup>31</sup> The pristine water fluxes of PSF; PSF/0.1% g-C<sub>3</sub>N<sub>4</sub>; PSF/0.2% g-C<sub>3</sub>N<sub>4</sub> and PSF/0.3% g-C<sub>3</sub>N<sub>4</sub> were determined at 25 bar using a dead-end filtration system, and the results are shown in Figure 9b, where the pristine water fluxes of PSF; PSF/0.1% g-C<sub>3</sub>N<sub>4</sub>; PSF/0.2% g-C<sub>3</sub>N<sub>4</sub> and PSF/0.3% g-C<sub>3</sub>N<sub>4</sub> are 26.8, 29.8, 44.0, and 54.4 L m<sup>-2</sup> h<sup>-1</sup>, respectively. The water flux for PSF/g-C<sub>3</sub>N<sub>4</sub> membrane increased from 29.8 to 54.4 L m<sup>-2</sup> h<sup>-1</sup> by the addition of g-C<sub>3</sub>N<sub>4</sub> from 0.1% to 0.3%. It is obvious that the introduction of g-C<sub>3</sub>N<sub>4</sub> promotes the formation of pores, which also creates large pore channels to maximize membrane flux. The increase in water flux that was noticed shows the importance of surface hydrophilicity on membrane flux as well as the increase in membrane pores caused by the addition of nanoparticles.<sup>38</sup> The increase in membrane flux is closely correlated with the hydrophilicity of the membrane materials. A similar result was found by Vatanpour et al.<sup>54</sup> membrane pore size and electrostatic interaction between the membrane surface and ions in solution, as well as nanochannels, influence the rejection of organic and inorganic pollutants from waste water.<sup>54</sup>

The COD experiment results for pristine PSF, PSF/0.1% g-C<sub>3</sub>N<sub>4</sub>, PSF/0.2% g-C<sub>3</sub>N<sub>4</sub>, and PSF/0.3% g-C<sub>3</sub>N<sub>4</sub> membranes are shown in Figure 10a, with COD removal

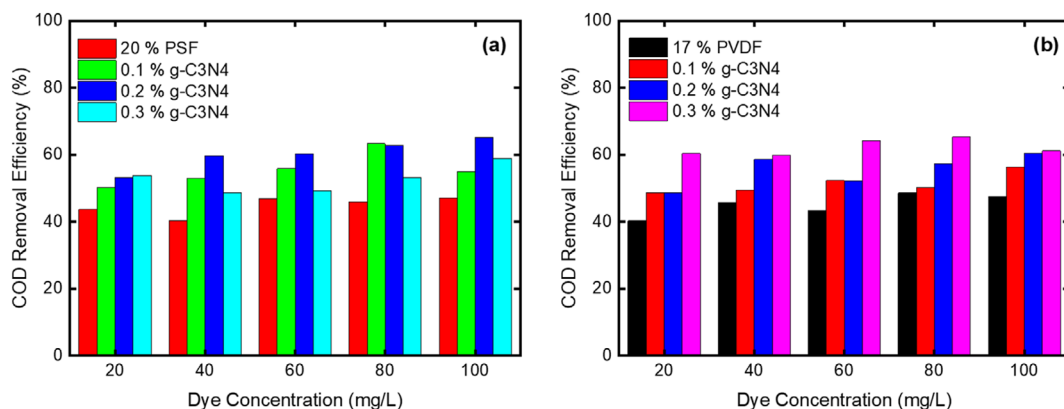


**FIGURE 10** Effect of dye concentration (20–100 mg/L) on COD removal efficiency for (a) pristine PSF and PSF/g-C<sub>3</sub>N<sub>4</sub> composite membranes, (b) pristine PVDF and PVDF/g-C<sub>3</sub>N<sub>4</sub> composite membranes. [Color figure can be viewed at [wileyonlinelibrary.com](https://onlinelibrary.wiley.com/doi/10.1002/app.54514)]

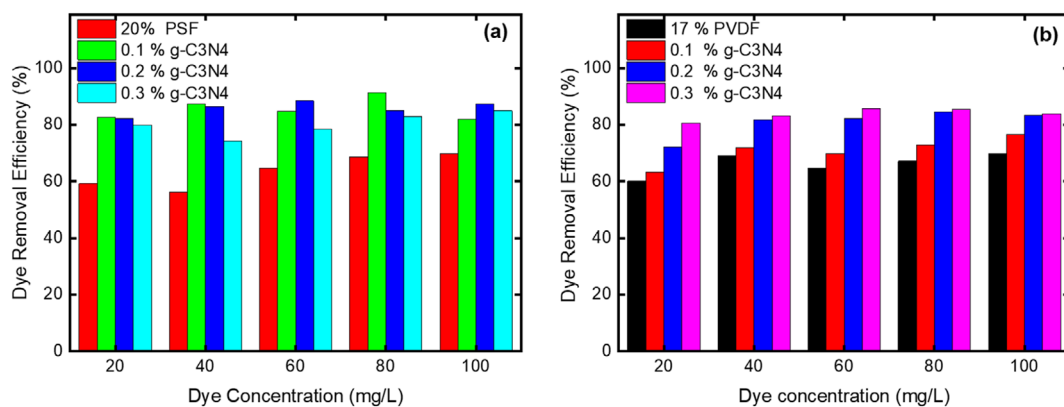


**FIGURE 11** Effect of RB5 concentration (20–100 mg/L) on removal efficiency (a) for pristine PSF and PSF/g-C<sub>3</sub>N<sub>4</sub> composite membranes, (b) for PVDF and PVDF/g-C<sub>3</sub>N<sub>4</sub> composite membranes. [Color figure can be viewed at [wileyonlinelibrary.com](https://onlinelibrary.wiley.com/doi/10.1002/app.54514)]

**TABLE 2** Comparison of hybrid membranes based on g-C<sub>3</sub>N<sub>4</sub> for the removal of organic dyes.

Membrane material	Dye	Concentration	Dye rejection %	COD rejection %	References
PVDF/SPPO/g-C <sub>3</sub> N <sub>4</sub>	MB	10 mg/L	100	–	55
	RhB		84		
	EB		89		
PES/GO/g-C <sub>3</sub> N <sub>4</sub>	EB	10 mg/L	95.5	–	56
HPEI/Gly-GO/g-C <sub>3</sub> N <sub>4</sub>	RhB	20 mg/L	77.7	–	43
	MB	20 mg/L	90		
PAA/g-C <sub>3</sub> N <sub>4</sub>	EB	10 mg/L	83.0	–	57
PVDF/g-C <sub>3</sub> N <sub>4</sub> /rGO/TiO <sub>2</sub>	MB	–	94.2	–	58
PVDF/g-C <sub>3</sub> N <sub>4</sub> /chitosan	Direct Blue 14	1–5 mg/L	93	–	31
PVDF/g-C <sub>3</sub> N <sub>4</sub>	Reactive Black 5	20–100 mg/L	85.6	65.3	This study
PSF/g-C <sub>3</sub> N <sub>4</sub>	Reactive Black 5	20–100 mg/L	91.3	65.1	This study

efficiency values for PSF/0.1% g-C<sub>3</sub>N<sub>4</sub>, PSF/0.2% g-C<sub>3</sub>N<sub>4</sub>, and PSF/0.3% g-C<sub>3</sub>N<sub>4</sub> membranes of more than 50%. Figure 10b shows the COD experiment findings for pristine PVDF, PVDF/0.1% g-C<sub>3</sub>N<sub>4</sub>, PVDF/0.2% g-C<sub>3</sub>N<sub>4</sub>, and PVDF/0.3% g-C<sub>3</sub>N<sub>4</sub> membranes. PVDF/0.1% g-C<sub>3</sub>N<sub>4</sub>,

PVDF/0.2% g-C<sub>3</sub>N<sub>4</sub>, and PVDF/0.3% g-C<sub>3</sub>N<sub>4</sub> membrane COD removal efficiency rates are more than 45%.

As can be seen in Figure 11a, the fabricated PSF/g-C<sub>3</sub>N<sub>4</sub> membranes showed high RB5 dye rejection, more than 80%. Especially, the membrane that contains

TABLE 3 Comparison of removal of reactive black 5 dye with different treatment methods.

Treatment methods	Concentration	Dye rejection %	COD rejection %	References
Membrane filtration (PAN(92)-co-P2EHA(8)-PANI(15%).	100 ppm	99.5	–	15
Adsorption (Chitosan)	30 ppm	85.0	–	59
Photocatalytic oxidation process (TiO <sub>2</sub> Catalyst)	400 ppm	98.7	–	60
Electrocoagulation	100 ppm	90	–	61
Electro-flocculation	90 ppm	66.43	–	62
Adsorption	100 ppm	87.63	–	63
Magnetic sedimentation (biocoagulant)	10–25 ppm	96.2	–	64
Coagulation/flocculation+UF	10 ppm	100	–	65
Ozonation and biological treatment	100 ppm	96.1	36,8	66
Fenton oxidation	120 ppm	99	–	67
Ultrafiltration ceramic membrane	50 ppm	79.8	–	68
	500 ppm	73.2		
Nanofiltration-electrodialysis	2–18 g/L	99.94	–	69
Membrane filtration (PVDF/ g-C <sub>3</sub> N <sub>4</sub> )	20–100 ppm	85.6	65.3	This study
Membrane filtration (PSF/ g-C <sub>3</sub> N <sub>4</sub> )	20–100 ppm	91.3	65.1	This study

0.1 wt% g-C<sub>3</sub>N<sub>4</sub> has a rejection of 91.3% for the RB5. The improved membrane hydrophilicity, which resulted in dye molecules being rejected from the membrane surface by hydrophobic repulsive forces. These forces are responsible for the improved the modified membranes dye separation performance.<sup>38</sup> As shown in Figure 11b, RB5rejection of the fabricated PVDF/g-C<sub>3</sub>N<sub>4</sub> membranes is more than 60%. Especially, the membrane containing 0.3 wt% g-C<sub>3</sub>N<sub>4</sub> has a rejection of 85.6% for 60 mg/L RB5concentration.

The RB5 rejection rate of various hybrid membranes made of graphene-based materials is summarized in Table 2. The various treatment techniques for removal of RB 5 dye are listed in Table 3. The majority of the research on treatability of dyes that is included below used wastewater that contained a particular dye as their main indicator of treatment effectiveness. However, many of these studies did not analyze COD and COD rejection form the wastewater. The effects of two different composite membranes on the efficiency of dye and COD rejection were examined and compared in this study.

## 4 | CONCLUSIONS

In this study, g-C<sub>3</sub>N<sub>4</sub> nanosheets were used to produce new ultrafiltration (UF) membranes manufactured of PVDF and PSF. For the removal of RB5 dye, the performance of the membranes was compared and evaluated.

In summary, we have successfully fabricated g-C<sub>3</sub>N<sub>4</sub> nanosheets embedded in PSF and PVDF membranes at three different concentrations. The effects of two different composite membranes on the efficiency of dye and COD rejection were examined and compared in detail. Because of the g-C<sub>3</sub>N<sub>4</sub> nanosheets has a large surface area and tunable pore size, which can effectively block the transport of RB5 dye molecules through the membrane It is also understood that PVDF/g-C<sub>3</sub>N<sub>4</sub> and PVDF/g-C<sub>3</sub>N<sub>4</sub> can change the surface properties of the membrane, making them more hydrophilic and reducing fouling. The g-C<sub>3</sub>N<sub>4</sub> nanosheets blended membranes showed better RB5 dye rejection than pristine PSF and PVDF membranes. The results of the experimental filtration showed that RB5 rejection reached maximum values of 91.3% for 0.1 wt% g-C<sub>3</sub>N<sub>4</sub>/PSF, and 85.6% for 0.3 wt% g-C<sub>3</sub>N<sub>4</sub>/PVDF. The differences in RB5 dye rejection between g-C<sub>3</sub>N<sub>4</sub> embedded in PVDF and PSF membranes were understood to be due to differences in the properties of these membranes. g-C<sub>3</sub>N<sub>4</sub>/PVDF membranes have a high affinity for hydrophobic substances and therefore, have higher RB5 dye rejection properties compared to g-C<sub>3</sub>N<sub>4</sub>/PSF membranes. 0.3 wt% g-C<sub>3</sub>N<sub>4</sub>/PVDF membrane demonstrates COD removal efficiency of 65.3% for a RB5 dye concentration of 60 mg/L. 0.1 wt% g-C<sub>3</sub>N<sub>4</sub>/PSF membrane shows a 65.1% COD removal efficiency for RB5 dye concentration of 80 mg/L. Overall, both g-C<sub>3</sub>N<sub>4</sub>/PVDF and g-C<sub>3</sub>N<sub>4</sub>/PSF membranes are effective in COD removal, making them suitable for RB5 dye rejection in water treatment applications.

## AUTHOR CONTRIBUTIONS

**Dilek Senol-Arslan:** Conceptualization (equal); investigation (lead); methodology (equal); writing – original draft (lead); writing – review and editing (lead). **Ayşe Gul:** Conceptualization (supporting); data curation (lead); writing – original draft (supporting); writing – review and editing (supporting). **Nadir Dizge:** Conceptualization (equal); supervision (lead); writing – original draft (equal); writing – review and editing (equal). **Kasim Ocakoglu:** Conceptualization (equal); data curation (supporting); methodology (lead); writing – original draft (equal); writing – review and editing (equal). **Nigmet Uzal:** Conceptualization (lead); data curation (equal); investigation (lead); methodology (lead); writing – original draft (equal); writing – review and editing (equal).

## CONFLICT OF INTEREST STATEMENT

The authors declare that there are no conflicts of interest.

## DATA AVAILABILITY STATEMENT

The data that support the findings of this study are available from the corresponding author upon reasonable request.

## ORCID

Dilek Senol-Arslan  <https://orcid.org/0000-0001-9639-2843>

## REFERENCES

- [1] S. Zinatloo-Ajabshir, S. A. Heidari-Asil, M. Salavati-Niasari, *Sep. Purif. Technol.* **2021**, 267, 118667.
- [2] S. Zinatloo-Ajabshir, M. Salavati-Niasari, *J. Mol. Liq.* **2017**, 243, 219.
- [3] M. Ghodrati, M. Mousavi-Kamazani, S. Zinatloo-Ajabshir, *Ceram. Int.* **2020**, 46, 28894.
- [4] M. Rezayeenik, M. Mousavi-Kamazani, S. Zinatloo-Ajabshir, *Appl. Phys. A* **2023**, 129, 47.
- [5] S. Zinatloo-Ajabshir, M. S. Morassaei, O. Amiri, M. Salavati-Niasari, L. K. Foong, *Ceram. Int.* **2020**, 46, 17186.
- [6] A. Zonarsaghar, M. Mousavi-Kamazani, S. Zinatloo-Ajabshir, *Ceram. Int.* **2021**, 47, 35248.
- [7] M. H. Esfahani, S. Zinatloo-Ajabshir, H. Naji, C. A. Marjerrison, J. E. Greedan, M. Behzad, *Ceram. Int.* **2023**, 49, 253.
- [8] A. Zonarsaghar, M. Mousavi-Kamazani, S. Zinatloo-Ajabshir, *Int. J. Hydrog. Energy* **2022**, 47, 5403.
- [9] P. K. Das, C. Mohanty, G. K. Purohit, S. Mishra, S. Palo, *Environ. Nanotechnol. Monit. Manag.* **2022**, 18, 100679.
- [10] A. A. Beni, H. Jabbari, *Results Eng.* **2022**, 15, 100467.
- [11] L. Pokrajac, A. Abbas, W. Chrzanowski, G. M. Dias, B. J. Eggleton, S. Maguire, E. Maine, T. Malloy, J. Nathwani, L. Nazar, A. Sips, J. Sone, A. van den Berg, P. S. Weiss, S. Mitra, *ACS Nano* **2021**, 15, 18608.
- [12] S. Zinatloo-Ajabshir, M. Emsaki, G. Hosseinzadeh, *J. Colloid Interface Sci.* **2022**, 619, 1.
- [13] S. Zinatloo-Ajabshir, M. S. Morassaei, M. Salavati-Niasari, *Compos. Part B* **2019**, 167, 643.
- [14] S. Zinatloo-Ajabshir, E. Shafaati, A. Bahrami, *Ceram. Int.* **2022**, 48, 24695.
- [15] L. Semiz, *Polym. Bull.* **2020**, 77, 3047.
- [16] M. R. Jalali Sarvestani, Z. Doroudi, *J. Water Environ. Nanotechnol.* **2020**, 5, 180.
- [17] I. Kolesnyk, J. Kujawa, H. Bubela, V. Konovalova, A. Burban, A. Cyganiuk, W. Kujawski, *Sep. Purif. Technol.* **2020**, 250, 117231.
- [18] Y. Cui, X. An, S. Zhang, Q. Tang, H. Lan, H. Liu, J. Qu, *Water Res.* **2021**, 200, 117207.
- [19] M. Ahmaruzzaman, S. R. Mishra, *Mater. Res. Bull.* **2021**, 143, 111417.
- [20] Hasanzade, P.; Gharbani, P.; Derakhshan, F.; Maher, B. M., **2021**.
- [21] B. Li, M. Meng, Y. Cui, Y. Wu, Y. Zhang, H. Dong, Z. Zhu, Y. Feng, C. Wu, *Chem. Eng. J.* **2019**, 365, 405.
- [22] P. Li, D. Zheng, M. Gao, X. Zuo, L. Sun, Q. Zhou, J. Lin, *ACS Appl. Energy Mater.* **2021**, 4, 8875.
- [23] X. Li, G. Huang, X. Chen, J. Huang, M. Li, J. Yin, Y. Liang, Y. Yao, Y. Li, *Sci. Total Environ.* **2021**, 792, 148462.
- [24] S. Saki, D. Senol-Arslan, N. Uzal, *J. Appl. Polym. Sci.* **2020**, 137, 49057.
- [25] S. Cheng, S. Zhao, B. Xing, Y. Liu, C. Zhang, H. Xia, *J. Cleaner Prod.* **2022**, 348, 131301.
- [26] X. Zhang, Z. Zong, X. Zhang, D. Zhang, Q. Luo, C. Bi, Y. Fan, *Polyhedron* **2020**, 191, 114816.
- [27] F. Mcyotto, Q. Wei, D. K. Macharia, M. Huang, C. Shen, C. W. Chow, *Chem. Eng. J.* **2021**, 405, 126674.
- [28] W. Zhang, H. Song, L. Zhu, G. Wang, Z. Zeng, X. Li, *J. Environ. Chem. Eng.* **2022**, 10, 107202.
- [29] K. Sunil, P. Sherugar, S. Rao, C. Lavanya, G. R. Balakrishna, G. Arthanareeswaran, M. Padaki, *J. Environ. Chem. Eng.* **2021**, 9, 106328.
- [30] U. Baig, M. Faizan, M. Sajid, *Chemosphere* **2021**, 282, 130898.
- [31] P. Hassanzadeh, P. Gharbani, F. Derakhshanfard, B. Memar Maher, *J. Polym. Environ.* **2021**, 29, 3693.
- [32] C. Lavanya, R. G. Balakrishna, *Sep. Purif. Technol.* **2020**, 230, 115887.
- [33] S. Ayazi, M. Ghorbani, R. Abedini, *Chem. Eng. Res. Des.* **2021**, 169, 214.
- [34] M. R. Mehrnia, Y. M. Mojtahedi, M. Homayoonfal, *Desalination* **2015**, 372, 75.
- [35] Y. Chen, G. Yang, B. Liu, H. Kong, Z. Xiong, L. Guo, G. Wei, *Chem. Eng. J.* **2022**, 430, 132721.
- [36] H. Ouaddari, A. Karim, B. Achiou, S. Saja, A. Aaddane, J. Bennazha, I. E. A. El Hassani, M. Ouammou, A. Albizane, *J. Environ. Chem. Eng.* **2019**, 7, 103268.
- [37] R. Goswami, M. Gogoi, A. Borah, H. Sarmah, P. G. Ingole, S. Hazarika, *Environ. Nanotechnol. Monit. Manag.* **2021**, 16, 100492.
- [38] M. Khansanami, A. Esfandiari, *Environ. Res.* **2021**, 201, 111576.
- [39] S. Sakarkar, S. Muthukumaran, V. Jegatheesan, *Chemosphere* **2020**, 257, 127144.
- [40] A. Modi, J. Bellare, *J. Water Process. Eng.* **2019**, 29, 100783.
- [41] P. Gharbani, A. Mehrizad, *Carbohydr. Polym.* **2022**, 277, 118860.
- [42] B. Sert, Y. Ozay, E. Harputlu, S. Ozdemir, M. S. Yalcin, K. Ocakoglu, N. Dizge, *Colloids Surf., A* **2021**, 623, 126571.

- [43] Z. Wu, L. Gao, J. Wang, F. Zhao, L. Fan, D. Hua, S. Japip, J. Xiao, X. Zhang, S.-F. Zhou, *J. Membr. Sci.* **2020**, *601*, 117948.
- [44] D. R. Paul, S. Gautam, P. Panchal, S. P. Nehra, P. Choudhary, A. Sharma, *ACS Omega* **2020**, *5*, 3828.
- [45] D. Saha, P. Gismondi, K. W. Kolasinski, S. L. Shumlas, S. Rangan, B. Eslami, A. McConnell, T. Bui, K. Cunfer, *Surf. Interfaces* **2021**, *26*, 101367.
- [46] S. P. Adhikari, H. R. Pant, H. J. Kim, C. H. Park, C. S. Kim, *Ceram. Int.* **2015**, *41*, 12923.
- [47] S. Pareek, M. Sharma, S. Lal, J. K. Quamara, *J. Mater. Sci. Mater. Electron.* **2018**, *29*, 13043.
- [48] F. Chang, J. Zhang, Y. Xie, J. Chen, C. Li, J. Wang, J. Luo, B. Deng, X. Hu, *Appl. Surf. Sci.* **2014**, *311*, 574.
- [49] Y. Cui, L. Yang, M. Meng, Q. Zhang, B. Li, Y. Wu, Y. Zhang, J. Lang, C. Li, *Korean J. Chem. Eng.* **2019**, *36*, 236.
- [50] N. Nikooe, E. Saljoughi, *Appl. Surf. Sci.* **2017**, *413*, 41.
- [51] L. D. Anbealagan, T. Y. S. Ng, T. L. Chew, Y. F. Yeong, S. C. Low, Y. T. Ong, C.-D. Ho, Z. A. Jawad, *Membranes* **2021**, *11*, 630.
- [52] M. Kim, S. Hwang, J.-S. Yu, *J. Mater. Chem.* **2007**, *17*, 1656.
- [53] J. Huang, J. Hu, Y. Shi, G. Zeng, W. Cheng, H. Yu, Y. Gu, L. Shi, K. Yi, *J. Colloid Interface Sci.* **2019**, *541*, 356.
- [54] V. Vatanpour, S. S. M. Khadem, A. Dehqan, S. Paziresh, M. R. Ganjali, M. Mehrpooya, E. Pourbasheer, A. Badieli, A. Esmaeili, I. Koyuncu, *J. Membr. Sci.* **2022**, *660*, 120893.
- [55] J. Ran, T. Pan, Y. Wu, C. Chu, P. Cui, P. Zhang, X. Ai, C. F. Fu, Z. Yang, T. Xu, *Am. Ethnol.* **2019**, *131*, 16615.
- [56] L. Liu, Y. Zhou, J. Xue, H. Wang, *AIChE J.* **2019**, *65*, e16699.
- [57] Y. Wang, L. Liu, J. Xue, J. Hou, L. Ding, H. Wang, *AIChE J.* **2018**, *64*, 2181.
- [58] K. Venkatesh, G. Arthanareeswaran, A. C. Bose, P. S. Kumar, *Sep. Purif. Technol.* **2020**, *241*, 116709.
- [59] M. Kamranifar, A. Rezaei, E. Taheri, N. Mengelizadeh, H. Pourzamani, *J. Rafsanjan Univ. Med. Sci.* **2017**, *15*, 929.
- [60] B. Gezer, R. Gezer, C. Gezer, İleri Mühendislik Çalışmaları ve Teknolojileri Dergisi *2*, 98.
- [61] O. Bediha, E. Beytullah, A. Özdemir, *Sakarya Univ. J. Sci.* **2020**, *24*, 712.
- [62] A. Ikhlaq, M. Zafar, F. Javed, A. Yasar, A. Akram, S. Shabbir, F. Qi, *Water Sci. Technol.* **2021**, *84*, 1943.
- [63] K. Archana, R. Rajagopal, R. Kavitha, V. G. Krishnaswamy, *Surf. Interfaces* **2022**, *29*, 101724.
- [64] C. S. Miyashiro, G. A. P. Mateus, T. R. T. Dos Santos, M. P. Paludo, R. Bergamasco, M. R. Fagundes-Klen, *Mater. Sci. Eng., C* **2021**, *119*, 111523.
- [65] N. D. C. L. Beluci, G. A. P. Mateus, C. S. Miyashiro, N. C. Homem, R. G. Gomes, M. R. Fagundes-Klen, R. Bergamasco, A. M. S. Vieira, *Sci. Total Environ.* **2019**, *664*, 222.
- [66] S. M. D. A. G. Ulson, K. A. S. Bonilla, A. A. U. de Souza, *J. Hazard. Mater.* **2010**, *179*, 35.
- [67] Y. Süzen, C. Ozmetin, *Desalination Water Treat.* **2019**, *172*, 106.
- [68] E. Alventosa-deLara, S. Barredo-Damas, E. Zuriaga-Agustí, M. I. Alcaina-Miranda, M. I. Iborra-Clar, *Sep. Purif. Technol.* **2014**, *129*, 96.
- [69] J. Lin, Q. Chen, X. Huang, Z. Yan, X. Lin, W. Ye, S. Arcadio, P. Luis, J. Bi, B. Van der Bruggen, *J. Hazard. Mater.* **2021**, *419*, 126505.

**How to cite this article:** D. Senol-Arslan, A. Gul, N. Dizge, K. Ocakoglu, N. Uzal, *J. Appl. Polym. Sci.* **2023**, *140*(41), e54514. <https://doi.org/10.1002/app.54514>